



# Plant uptake of CO<sub>2</sub> outpaces losses from permafrost and plant respiration on the Tibetan Plateau

Da Wei<sup>a,1</sup>, Yahui Qi<sup>a,b,1</sup>, Yaoming Ma<sup>b,c</sup>, Xufeng Wang<sup>d</sup>, Weiqiang Ma<sup>c</sup>, Tanguang Gao<sup>e</sup>, Lin Huang<sup>f</sup>, Hui Zhao<sup>a</sup>, Jianxin Zhang<sup>a,b</sup>, and Xiaodan Wang<sup>a,2</sup>

<sup>a</sup>Institute of Mountain Hazards and Environment, Chinese Academy of Sciences, Chengdu 610041, China; <sup>b</sup>College of Resources and Environment, University of Chinese Academy of Sciences, Beijing 100049, China; <sup>c</sup>Institute of Tibetan Plateau Research, Chinese Academy of Sciences, Beijing 100101, China; <sup>d</sup>Northwest Institute of Eco-Environment and Resources, Chinese Academy of Sciences, Lanzhou, 730000, China; <sup>e</sup>College of Earth and Environmental Sciences, Lanzhou University, Lanzhou 730000, China; and <sup>f</sup>Institute of Geophysical Science and Natural Resource Research, Chinese Academy of Sciences, Beijing 100101, China

Edited by Steven C. Wofsy, Harvard University, Cambridge, MA, and approved June 7, 2021 (received for review August 22, 2020)

**High-latitude and high-altitude regions contain vast stores of permafrost carbon. Climate warming may result in the release of CO<sub>2</sub> from both the thawing of permafrost and accelerated autotrophic respiration, but it may also increase the fixation of CO<sub>2</sub> by plants, which could relieve or even offset the CO<sub>2</sub> losses. The Tibetan Plateau contains the largest area of alpine permafrost on Earth. However, the current status of the net CO<sub>2</sub> balance and feedbacks to warming remain unclear, given that the region has recently experienced an atmospheric warming rate of over 0.3 °C decade<sup>-1</sup>. We examined 32 eddy covariance sites and found an unexpected net CO<sub>2</sub> sink during 2002 to 2020 (26 of the sites yielded a net CO<sub>2</sub> sink) that was four times the amount previously estimated. The CO<sub>2</sub> sink peaked at an altitude of roughly 4,000 m, with the sink at lower and higher altitudes limited by a low carbon use efficiency and a cold, dry climate, respectively. The fixation of CO<sub>2</sub> in summer is more dependent on temperature than the loss of CO<sub>2</sub> than it is in the winter months, especially at higher altitudes. Consistently, 16 manipulative experiments and 18 model simulations showed that the fixation of CO<sub>2</sub> by plants will outpace the loss of CO<sub>2</sub> under a wetting-warming climate until the 2090s (178 to 318 Tg C y<sup>-1</sup>). We therefore suggest that there is a plant-dominated negative feedback to climate warming on the Tibetan Plateau.**

permafrost | carbon | climate change | eddy covariance | Tibetan Plateau

**H**igh-latitude and high-altitude regions have a harsh, cold climate that favors the storage of carbon (C) in the entire soil column, including the permafrost layer (1). This permafrost contains the largest store of C in terrestrial ecosystems (roughly 1,320 Pg C) (2). These cold ecosystems have experienced a much greater rate of climate warming (0.3 °C decade<sup>-1</sup>) than the 0.12 °C decade<sup>-1</sup> of warming across the global land surface as a whole (3). Warming can result in the release of CO<sub>2</sub> from the permafrost layer (4–6) but can also lead to increased fixation of CO<sub>2</sub> by plants (7–9), which can relieve or even offset the loss of CO<sub>2</sub> from permafrost.

The frozen soils in the high-latitude Arctic have experienced a warming rate of the permafrost ground temperature of 0.39 °C decade<sup>-1</sup> (10). This has affected the permafrost reserves of C, as well as plant growth (7), and may also provide a feedback to climate warming, although the direction and magnitude of this feedback are still highly uncertain (5, 8, 9). Tundra ecosystems might be a net CO<sub>2</sub> source as a result of the differential amplification of the C cycle under warming conditions (11)—that is, winter CO<sub>2</sub> losses are more temperature-sensitive than the uptake of CO<sub>2</sub> by plants during the growing season. A recent study showed that the Pan-Arctic permafrost is a net CO<sub>2</sub> source of 630 Tg C y<sup>-1</sup> (12), albeit with strong uncertainties (range: 15 to 975 Tg C y<sup>-1</sup>). By contrast, a synthesis study and model simulations reported that the Arctic can act as a CO<sub>2</sub> sink at the ecosystem level (8, 13, 14), given that the uptake of CO<sub>2</sub> by plants is accelerating as a result of Arctic greening. These contrasting results reveal the large uncertainties in feedbacks to the present-day warming climate across Arctic permafrost ecosystems.

High-altitude mountains also have vast regions of permafrost (15), but less is known about the CO<sub>2</sub> balance in these regions and its variation in the Earth's currently changing climate. The Tibetan Plateau ranges from <3,000 to 8,844 m in altitude and is the largest region of alpine permafrost on Earth, contributing 10% to the global store of permafrost C (*SI Appendix, Fig. S1*) (16, 17). Continuous permafrost covers 84.2 million hectares of the Tibetan Plateau, discontinuous permafrost covers 15.9 million hectares, and isolated permafrost covers 23.0 million hectares (16, 17). The Tibetan Plateau has experienced climate warming of 0.3 °C decade<sup>-1</sup> in the atmospheric temperature and an increase in precipitation since the 1960s (18). In situ observations and simulations both suggest a significant increase in the ground temperature of 0.4 °C decade<sup>-1</sup> over the last 50 y, causing extensive thawing of the permafrost (19–21). High-resolution observations from remote sensing satellites and unmanned aerial vehicles have shown an acceleration in thaw slumps and thermokarst lakes (22, 23), although on relatively small scales (a few hundred meters to several kilometers). The thawing of permafrost may have affected the regional CO<sub>2</sub> balance by causing large losses of CO<sub>2</sub>. In situ observations at thaw slumps, incubation experiments, and numerical modeling have all shown that permafrost is highly vulnerable to warming on the Tibetan

## Significance

**Cold regions contain vast stores of permafrost carbon. Rapid warming will cause permafrost to thaw and plant respiration to accelerate, with a resultant loss of CO<sub>2</sub>, but could also increase the fixation of CO<sub>2</sub> by plants. A network of 32 eddy covariance sites on the Tibetan Plateau, which has the largest store of alpine permafrost carbon on Earth, shows that this region functions as a net CO<sub>2</sub> sink. Our sensitivity analyses, experiments, and model simulations consistently showed that the fixation of CO<sub>2</sub> by plants outpaces the loss of CO<sub>2</sub> from permafrost and accelerates plant respiration. This indicates a plant-dominated CO<sub>2</sub> balance on the Tibetan Plateau, which could provide a negative feedback to climate warming.**

Author contributions: D.W. and Xiaodan Wang designed research; D.W. performed research; D.W., Y.Q., Y.M., Xufeng Wang, W.M., T.G., L.H., H.Z., J.Z., and Xiaodan Wang analyzed data; D.W. and Xiaodan Wang wrote the paper; Y.M., Xufeng Wang, W.M., and L.H. acquired data; and Y.M., Xufeng Wang, W.M., T.G., L.H., H.Z., and J.Z. discussed the results.

The authors declare no competing interest.

This article is a PNAS Direct Submission.

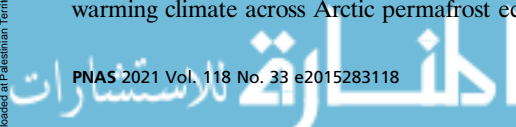
This open access article is distributed under [Creative Commons Attribution-NonCommercial-NoDerivatives License 4.0 \(CC BY-NC-ND\)](https://creativecommons.org/licenses/by-nc-nd/4.0/).

<sup>1</sup>D.W. and Y.Q. contributed equally to this work.

<sup>2</sup>To whom correspondence may be addressed. Email: wxd@imde.ac.cn.

This article contains supporting information online at <https://www.pnas.org/lookup/suppl/doi:10.1073/pnas.2015283118/-DCSupplemental>.

Published August 9, 2021.



Plateau (24–26). A recent model simulation predicted an 8% loss of C from permafrost soils by the end of the present century (25). However, repeated sampling surveys in the 2000s and 2010s suggested there has been an accumulation of soil C in these permafrost regions, largely due to increased plant growth (6), which strongly contradicts the conclusions of model simulations.

Many studies, especially those using remote sensing observations, have shown that the Tibetan Plateau is becoming greener under the currently warming and wetting climate and reduced density of grazing animals (27–30), suggesting a higher input of plant C to the soils. These contrasting views—that is, the model-based projection of the loss of CO<sub>2</sub> from permafrost and the inventory-based accumulation of soil C and satellite-based observations of increased vegetation—mean that it is unclear whether the CO<sub>2</sub> balance has been altered by the changing climate on the Tibetan Plateau. The size of the net CO<sub>2</sub> sink of the alpine ecosystems on the Tibetan Plateau is not yet fully understood, and the large-scale patterns of CO<sub>2</sub> flux are still unknown. It is therefore a research priority to investigate how the release of CO<sub>2</sub> from alpine permafrost might affect the CO<sub>2</sub> balance on the Tibetan Plateau.

Eddy covariance observations, owing to their high temporal resolution and landscape-scale coverage, are an ideal approach to the direct measurement of the exchange of CO<sub>2</sub>. Eddy covariance observations can therefore be used to assess the status and variation of the CO<sub>2</sub> balance of permafrost regions; however, historically, the establishment of eddy covariance sites on the Tibetan Plateau has

been rare and synthesis efforts limited. In this paper, we present an eddy covariance dataset covering 32 sites across the main alpine ecosystems of the Tibetan Plateau (Fig. 1, *SI Appendix*, *Figs. S2 and S3*, and *Datasets S1 and S2*), ranging from 3,000 to over 5,000 m in altitude during the period 2003 to 2019. We then analyze the drivers of the spatial pattern, with specific emphasis on the altitude-dependent pattern given the importance of altitudinal variation to high mountains like the Tibetan Plateau. The eddy covariance dataset was used to constrain a process-based model and project future changes in the CO<sub>2</sub> balance under the Representative Concentration Pathways (RCP) 2.6 to 8.5 scenarios using temperature and precipitation projections from 18 Coupled Model Intercomparison Project Phase 5 (CMIP5) models. To provide ground-based evidence about the feedback of the CO<sub>2</sub> balance of the alpine permafrost regions to warming, we also explored how the exchange of CO<sub>2</sub> reacts to changes in climate by examining 16 manipulated experiments across the Tibetan Plateau. By connecting the eddy covariance datasets, the process-based model, and the experiments, we aim to understand whether the Tibetan Plateau currently acts, and will continue to act, as a CO<sub>2</sub> sink under a rapidly changing climate.

## Results and Discussion

**Net CO<sub>2</sub> Sink across the Alpine Permafrost Regions.** Of the 32 eddy covariance sites during 2002 to 2020 across the alpine ecosystems, 26 reported a net CO<sub>2</sub> sink (*SI Appendix*, *Table S1* and *Figs. S2*

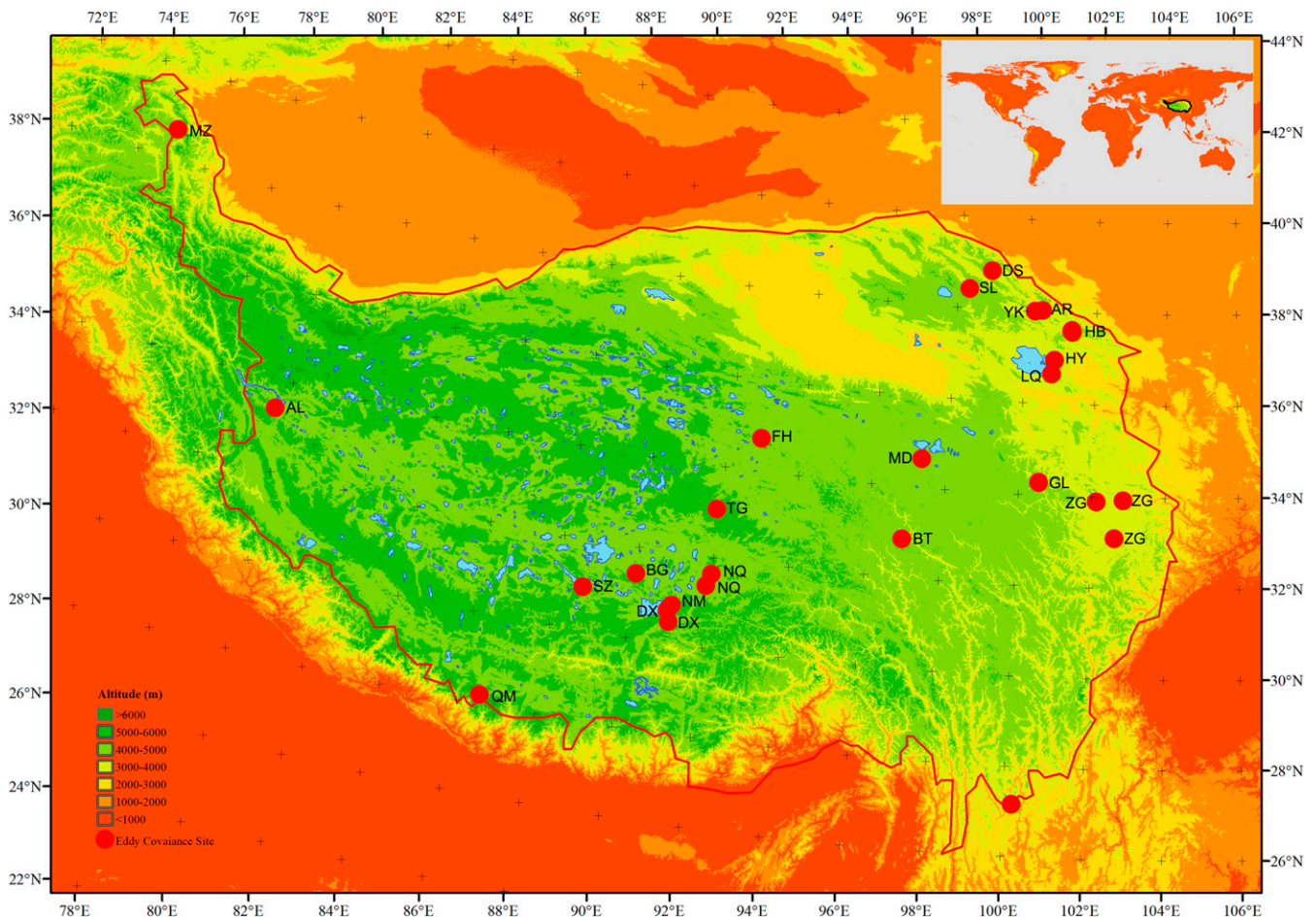


**Fig. 1.** Location of the 32 eddy covariance observation sites on the Tibetan Plateau. The inset map shows the location of the Tibetan Plateau (denoted by the black line). The characters in each solid circle are the name of each eddy covariance site: BT, Batang; DX, Dangxiong; DS, Dashalong; QM, Mt Qomolangma (Everest); GL, Guoluo; HB, Haibei; LQ, La. Qinghai; HY, Haiyan; FH, Fenghuoshan; LJ, Lijiang; MZ, Muztag; MD, Maduo; NM, NamCo; NQ, Naqu; SL, Shule; SZ, Shenzha; TG, Tanggula; YK, Yakou; ZG, Zoige.

and S3). The CO<sub>2</sub> exchange showed strong interannual variability (16 sites with multiyear observations); that is, 4 sites varied from a CO<sub>2</sub> sink to a source from year to year, while 12 sites showed a consistent net CO<sub>2</sub> sink across years. The alpine marshlands had the highest net ecosystem productivity (NEP) of  $104.7 \pm 59.0 \text{ g C m}^{-2} \text{ y}^{-1}$  ( $n = 9$ ), followed by alpine meadows ( $98.6 \pm 28.8 \text{ g C m}^{-2} \text{ y}^{-1}$ ,  $n = 15$ ), alpine steppes ( $64.3 \pm 38.7 \text{ g C m}^{-2} \text{ y}^{-1}$ ,  $n = 6$ ), and alpine shrublands ( $53.9 \pm 13.2 \text{ g C m}^{-2} \text{ y}^{-1}$ ,  $n = 2$ ) (Fig. 2A). Both the continuous and noncontinuous permafrost were net CO<sub>2</sub> sinks, and there was no significant difference between them (continuous permafrost:  $135.9 \pm 46.8 \text{ g C m}^{-2} \text{ y}^{-1}$ ,  $n = 10$ ; noncontinuous permafrost:  $72.3 \pm 23.9 \text{ g C m}^{-2} \text{ y}^{-1}$ ,  $n = 22$ ). We compared the results from the eddy covariance dataset with two independent datasets:

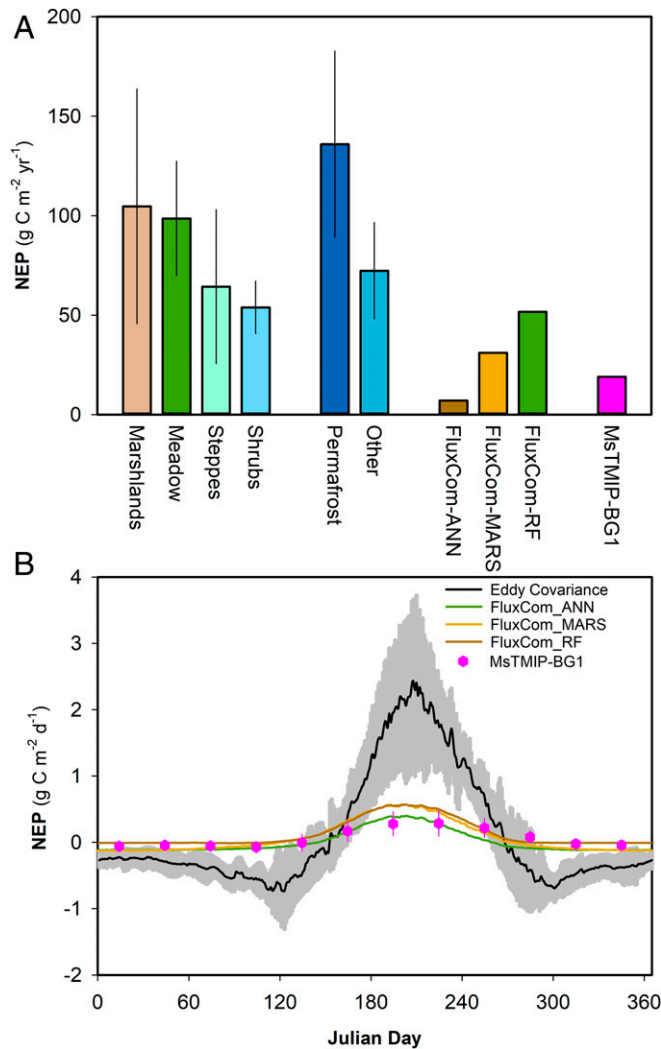


**Fig. 2.** Magnitude and seasonal variation of the net CO<sub>2</sub> sink. Comparison of average NEP observations across the Tibetan Plateau based on eddy covariance observations (32 sites covering all alpine ecosystem types), the FluxCom dataset, and the MsTMIP simulations with respect to their (A) magnitude and (B) seasonal variation. In A, the straight line in each bar indicates SE. "Permafrost" indicates continuous permafrost, while "other" indicates discontinuous, isolated, and sporadic permafrost. In B, the solid curve is the ensemble mean of 14 models of MsTMIP SG1, and the gray shading represents their 95% confidence band. The SG1 of MsTMIP is used in this study and is driven by various climate factors, N deposition, CO<sub>2</sub> enrichment, and changes in land use, including 14 modes (CLASS-CTEM-N, CLM4, CLM4VIC, DLEM, GTEC, ISAM, LPJ-wsl, ORCHIDEE-LSCE, SiB3, SiBCASA, TEM6, TRIPLEX-GHG, VEGAS2.1, and VISIT).

the machine learning FluxCom dataset (31) and the Multiscale Synthesis and Terrestrial Model Intercomparison Project (MsTMIP) (32). Both the FluxCom and MsTMIP datasets reported a net CO<sub>2</sub> sink, although the FluxCom dataset estimated a range from 7.09 to  $51.7 \text{ g C m}^{-2} \text{ y}^{-1}$ , and the MsTMIP dataset reported  $19.0 \text{ g C m}^{-2} \text{ y}^{-1}$  in the early twenty-first century, indicating a severe underestimation of the CO<sub>2</sub> sink of alpine ecosystems across the Tibetan Plateau. With respect to the seasonal variation, the winter losses of CO<sub>2</sub> were only one-third of the summer gain in CO<sub>2</sub> (SI Appendix, Fig. S4), based upon the eddy covariance dataset. The eddy covariance dataset also revealed a net CO<sub>2</sub> loss during the early and late growing seasons, although this was not captured by either the FluxCom or MsTMIP dataset (Fig. 2B).

The net CO<sub>2</sub> balance of the Tibetan Plateau has long been unknown owing to a lack of ground-based estimations. Several previous simulations have reported contradictory results (25, 33–36). Ground-based CO<sub>2</sub> exchange observations were not available at the time of those studies to adequately evaluate the models for this region. We used 32 in situ eddy covariance observations to quantify that the alpine ecosystems functioned as a net CO<sub>2</sub> sink, which is an observation-based evaluation of the CO<sub>2</sub> balance of the Tibetan Plateau. The net CO<sub>2</sub> sink of the Tibetan Plateau is roughly one-third the size of that of subtropical and temperate forests (37). This is an efficient CO<sub>2</sub> sink considering the gross primary productivity (GPP) of only  $676.8 \pm 121.0 \text{ g C m}^{-2} \text{ y}^{-1}$  of alpine ecosystems (37). Using the representative spatial extent of the main vegetation types across the Tibetan Plateau (67.5 million hectares [Mha] of alpine meadow, 71.9 Mha of alpine steppe, 6.32 Mha of alpine marshland [wetlands], and 19.7 Mha of alpine shrublands; deserts excluded due to data scarcity) (38), the CO<sub>2</sub> sink of the Tibetan Plateau was estimated to be  $130.0 \pm 53.6 \text{ Tg C y}^{-1}$  during the period 2003 to 2019.

It is still notable that uncertainty remains regarding the data coverage; for example, there is a lack of data in the depopulated deserts and barrens in the western and northern Tibetan Plateau, where observation is still challenging. These alpine deserts and barrens are generally higher in altitude and far from Indian Monsoon, resulting in a cold, dry climate and limiting plant growth and soil carbon accumulation (SI Appendix, Fig. S5). The fact that alpine deserts and barrens are low in carbon storage (biomass and soil carbon content) indicates that alpine deserts and barrens may play a minor role in regional CO<sub>2</sub> balance. A lack of long-term observation may also add uncertainty to our calculation, despite about half of the sites providing only 1 y of data. Our estimate is four times that of previous studies and the FluxCom and MsTMIP datasets (average for eight studies:  $35.2 \pm 10.5 \text{ Tg C y}^{-1}$ ; SI Appendix, Table S2) (33–36). Notably, the FluxCom dataset covers only two sites on the Tibetan Plateau (Haibei and Dangxiong), which may have reduced its ability to capture the CO<sub>2</sub> fluxes in this region. The strong solar radiation in these high mountains may have led to the considerable net CO<sub>2</sub> sink of these alpine ecosystems. The cold constraint on the loss of CO<sub>2</sub> during the winter may also favor the preservation of plant-fixed C—that is, the winter losses of CO<sub>2</sub> are only one-third of the summer gain in CO<sub>2</sub>. This is much lower than a recent study in the northern permafrost, suggesting that winter losses might be higher than the summer plant uptake of CO<sub>2</sub> (12), albeit with a large uncertainty.

**Spatial Pattern of the Net CO<sub>2</sub> Sink.** The net CO<sub>2</sub> sink across the alpine permafrost region showed a strong dependence on altitude, rather than latitude. Both the GPP and ecosystem respiration showed a negative correlation with altitude (SI Appendix, Fig. S6A and B), given they are highly correlated with each other (SI Appendix, Fig. S7). Both the altitude-dependent pattern of the GPP and ecosystem respiration are negatively correlated with the soil water content (SWC) (SI Appendix, Figs. S8 and S9). However, in contrast with our expectations, the NEP was strongest at about 4,000 m altitude (Fig. 3A). The unique altitudinal pattern of the

NEP altitudes was partly explained by the mean annual temperature (*SI Appendix, Figs. S8–S10*). It is well known that the growth of plants in very high mountain areas (altitudes >4,000 m) is limited by the cold climate and supply of nutrients (e.g., available nitrogen). For sites at lower altitudes and with a warmer climate (altitudes <4,000 m), we assumed that the respiration of both plants and soils in the warmer environment may have consumed a large portion of the C, resulting in a lower carbon use efficiency (CUE = NEP/GPP). Further analyses of the CUE along lines of altitude supported this suggestion by showing a positive increase in the CUE with increasing altitude (Fig. 3B). Analyses also suggested that the temperature sensitivity of winter CO<sub>2</sub> losses across different sites has a negative correlation with altitude (*SI Appendix, Fig. S11*). There is a prevailing pattern in which the uptake of CO<sub>2</sub> in summer is more sensitive to warming ( $Q_{10} = 1.54$ ) than the loss

of CO<sub>2</sub> during long, dry winters ( $Q_{10} = 1.33$ ). The difference between summer and winter temperature sensitivities shows a clear positive correlation with altitude, which explains the positive correlation between the CUE and altitude, which may have affected the altitudinal pattern of the NEP on the Tibetan Plateau.

The altitudinal gradient in mountain areas is always correlated with variations in climate, soil texture and nutrients, the growth of vegetation, and microbial activity (39). For the Tibetan Plateau, ground- (40) and satellite-based (41) observations have documented the variation in plant growth with altitude across the plateau, and it has long been recognized that the growth of vegetation—that is, the above-ground net primary productivity—is higher in the warmer and wetter areas at lower altitudes. We found a unique altitude-dependent pattern of the net CO<sub>2</sub> sink (NEP), challenging the assumption of a linear relationship between the NEP and altitude. Although there have been numerous studies of the latitudinal pattern of the NEP (37), our study recognizes an altitude-dependent pattern for the net CO<sub>2</sub> sink. The altitude-dependent pattern of the NEP along altitudinal gradients is similar to the broad-scale pattern along latitudinal gradients (*SI Appendix, Fig. S12*)—that is, the midaltitude CO<sub>2</sub> sink of alpine ecosystems is similar to the stronger midlatitude CO<sub>2</sub> sink. The NEP of tropical and boreal forests may be limited by respiration consumption and a cold climate, respectively (37).

**Net CO<sub>2</sub> Sink under a Warming and Wetting Climate.** In addition to the generally higher sensitivity to temperature of the summer CO<sub>2</sub> gain than the winter CO<sub>2</sub> loss, we explored the response of the net CO<sub>2</sub> sink to experimental warming by examining 16 short-term manipulated experiments across the Tibetan Plateau (*SI Appendix, Table S3 and Figs. S13 and S14*). The results verified a general benefit of warming to the net CO<sub>2</sub> sink, although it was found that warming >2 °C reduced the NEP relative to the control (Fig. 4A). Notably, 2 °C is roughly the warming predicted to be seen by the end of the present century with the present rate of warming of 0.26 °C decade<sup>-1</sup> under a business-as-usual scenario. The SWC determines the threshold and altitudinal pattern with respect to the effect of warming on the NEP (Fig. 4B)—that is, warming of dry soils (SWC <20%) reduces the CO<sub>2</sub> sink, whereas the warming of wetter soils (>20%) increases the CO<sub>2</sub> sink. The wetter soils are mainly alpine marshlands or meadows (at lower altitudes in the eastern Tibetan Plateau), whereas the drier soils correspond to alpine steppes and deserts (at much higher altitudes in the central and western Tibetan Plateau). There is a clear ecosystem-dependent pattern of the response of the NEP to warming (Fig. 4C), in which the growth of plants on alpine steppes at very high altitudes (>4,500 m altitude) is affected by limitations of soil water supply and thus a reduction in the NEP, whereas the NEP of alpine meadows and alpine marshlands at lower altitudes benefits from warming. Our experimental studies highlight the role of the SWC in determining the variation in the NEP under a future warming climate. However, there is a significant increase in precipitation (*SI Appendix, Fig. S15*), especially in the central and western Tibetan Plateau, which may compensate for the warming-induced drought and favor plant growth (42, 43).

We explored the variation in the CO<sub>2</sub> balance using CMIP5 model simulations under the RCP 2.6 to RCP 8.5 (Fig. 5) after constraint by the eddy covariance dataset (*SI Appendix, Figs. S16–S18*). The warming–wetting climate resulted in a net rate of increase in the NEP of 3.71 Tg C y<sup>-2</sup> during the past four decades and a net CO<sub>2</sub> sink of 152.4 ± 30.3 Tg C y<sup>-1</sup> in the early twenty-first century (2000 to 2018), generally consistent with the estimate based on eddy covariance observations during the same period. Future temperatures would increase by 1.5 to 5.5 °C by the 2090s, while precipitation would increase by 30 to 80 mm compared with the baseline period (2006 to 2015)—that is, the Tibetan Plateau would experience a continuously warming–wetting climate. It is not surprising that the net CO<sub>2</sub> sink of the Tibetan Plateau would

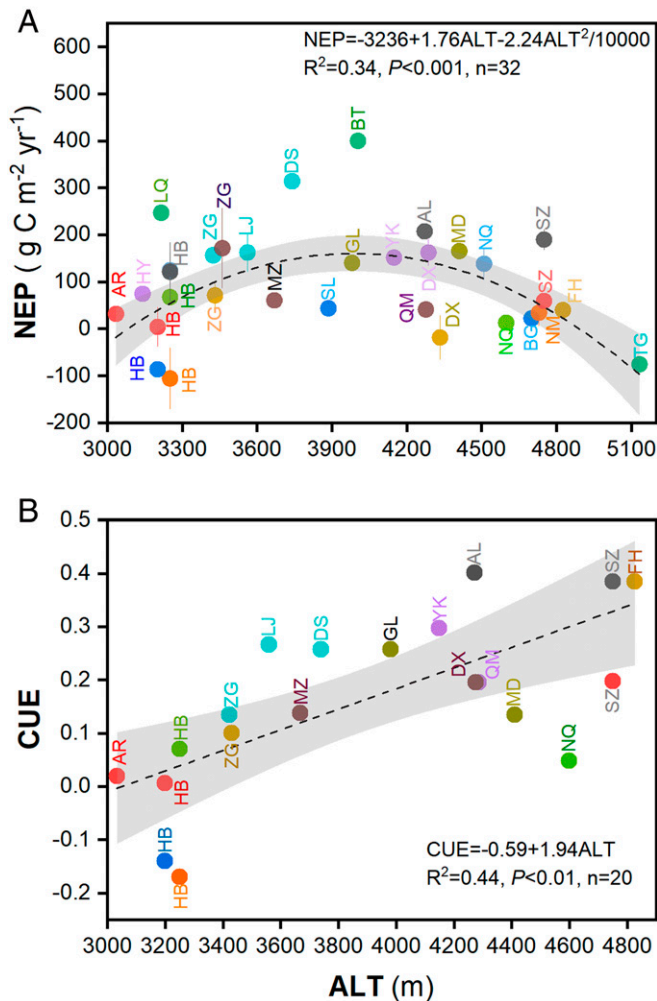


**Fig. 3.** Variation in CO<sub>2</sub> exchange with altitude across the Tibetan Plateau: (A) NEP, and (B) CUE = NEP/GPP. Each point is for one station, and the error bars indicate the interannual variability. The dashed lines indicate the hyperbola fit for the NEP and the linear fit for the CUE, while the gray shading represents the 95% confidence band of the fits. The fits are performed by weighting their variability (SD).  $P < 0.001$  in A indicates that the alternative hypothesis should be accepted (nonlinear relationship between NEP and altitude), and  $P < 0.01$  in B indicates that the alternative hypothesis should be accepted (linear relationship between CUE and altitude). ALT, altitude; AL, Ali; AR, Arou; BG, Ban'ge; BT, Batang; DX, Dangxiong; DS, Dshalong; QM, Mt Qomolangma (Everest); GL, Guoluo; HB, Haibei; LQ, La. Qinghai; HY, Haiyan; FH, Fenghuoshan; LJ, Lijiang; MZ, Muztag; MD, Maduo; NM, NamCo; NQ, Naqu; SL, Shule; SZ, Shenzha; TG, Tanggula; YK, Yakou; ZG, Zoige.

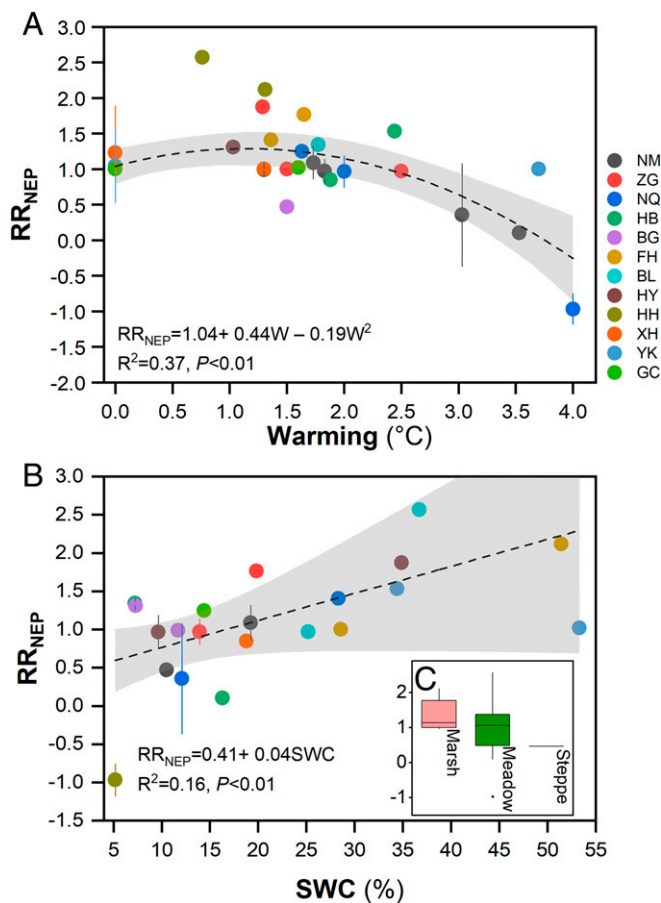


**Fig. 4.** Response of CO<sub>2</sub> exchange to experimental warming. (A) Response ratio of NEP ( $RR_{NEP}$ ) to the warming rate across 16 manipulated warming experiments on the Tibetan Plateau.  $RR_{NEP} = NEP_{Warming}/NEP_{Control}$ .  $RR_{NEP} > 1.0$  indicates a positive effect of warming on the NEP, while  $RR_{NEP} < 1.0$  indicates the opposite ( $RR_{NEP} < 0$  suggests that the warming has changed a net CO<sub>2</sub> sink of an ecosystem to a net CO<sub>2</sub> source). (B) Controls of SWC on the  $RR_{NEP}$  across the warming experiments on the Tibetan Plateau. (C) Ecosystem dependence on  $RR_{NEP}$  under warming. Each point in the figure represents a treatment for each site, which may include 3 to 10 replicates. The dashed lines indicate nonlinear or linear fits, with a Bayesian linear mixed effect model using the Markov chain Monte–Carlo sampling method. The SD of each treatment is used for weighting during the nonlinear and linear fitting. The gray shading represents the 95% confidence band of the fit.  $P < 0.01$  in A indicates that the alternative hypothesis should be accepted (nonlinear relationship between NEP and altitude), and  $P < 0.01$  in B indicates that the alternative hypothesis should be accepted (linear relationship between CUE and altitude). NM, NamCo; ZG, Zoige; NQ, Naqu; HB, Haibei; BG, Ban’ge; FH, Fenghuoshan; BL, Beiluhe; YH, Haiyan; HH, Heihe; XH, Xiaohupo; YK, Yikewulan; GC, Gangcha; CUE, carbon use efficiency (NEP/GPP).

increase under all scenarios, although the magnitudes differ. At the end of the current century, the NEP sink would increase to 178.1 to 317.9 Tg C y<sup>-1</sup> from RCP 2.6 to RCP 8.5. However, under RCP 8.0, the NEP reaches a steady state when warming exceeds 3.0 °C after the 2070s, largely due to a decrease in plant growth and the loss of too much CO<sub>2</sub> from permafrost and plant respiration.

The sensitivity analyses, manipulated field experiments, and model simulations all consistently show that the fixation of CO<sub>2</sub> by plants outpaces the potential loss of CO<sub>2</sub> from permafrost and accelerated plant respiration in current conditions. The fixation of CO<sub>2</sub> by vegetation has also led to an accumulation of soil CO<sub>2</sub> (6) in the surface layers across the Tibetan Plateau, as shown by <sup>137</sup>Cs–<sup>14</sup>C dating (44, 45), <sup>137</sup>Cs–<sup>140</sup>Pb<sub>ex</sub> dating (46), and a repeat-sampling approach (6), reporting a net soil C accumulation of 25 to

113 g C m<sup>-2</sup> y<sup>-1</sup>. Together, these methods have reported an average net soil C accumulation rate of 53.6 g C m<sup>-2</sup> y<sup>-1</sup> based upon isotope dating, indicating that roughly half of the C newly fixed by plants is stored in soils. These results show a general warming-induced CO<sub>2</sub> gain, rather than a net CO<sub>2</sub> loss, although too much warming under RCP 8.5 would cause a hiatus in the increase of plant growth and the NEP (36).

**Implications.** High-altitude and high-latitude regions have a vast permafrost store of C and have experienced warming of 0.3 °C decade<sup>-1</sup>, much higher than the global average of 0.12 °C decade<sup>-1</sup> (3), which affects the permafrost reserves of C (7). The loss of CO<sub>2</sub> from permafrost and plant respiration is expected to change the net CO<sub>2</sub> balance in these regions, although the direction and magnitude remain uncertain. By examining 32 eddy covariance sites across all the alpine ecosystems of the Tibetan Plateau, the largest region of alpine permafrost on Earth, we found an unexpected net CO<sub>2</sub> sink. The evidence (i.e., the higher temperature sensitivities of summer CO<sub>2</sub> uptake than winter CO<sub>2</sub> loss, the net CO<sub>2</sub> gain following experimental warming, and 18 model simulations under various RCPs) consistently points to a net CO<sub>2</sub> gain under the current and future changing climate across the alpine permafrost on the Tibetan Plateau (Fig. 6). The manipulated warming experiments highlight the role of soil water in determining the response of the net C sink to warming considering the strong radiation in such a high-altitude region. The importance of soil water in determining the response of the NEP to warming was verified by comparing the manipulated experiments (>2 °C) and the model simulations and showed that warming-only would cause a loss of NEP induced by a water deficit, whereas warming–wetting would benefit the NEP (Fig. 6 B and C). The boost to plant growth in the warming–wetting climate of the Tibetan Plateau outpaces the loss of CO<sub>2</sub> from thawing permafrost and plant respiration, indicating a plant-dominated negative feedback in the alpine permafrost on the Tibetan Plateau. This study is distinctly different from a recent report predicting that the thawing of permafrost could potentially turn the region into a significant CO<sub>2</sub> source (25), which may be due to a lack of knowledge about plant C fixation under a warmer and wetter climate.

Additional work on observations and simulations would help to better characterize the variation and mechanisms affecting the net CO<sub>2</sub> balance of these alpine permafrost regions. More eddy covariance observations in the hinterland of the Tibetan Plateau (i.e., the interior of the Tibetan Plateau) in the near future would better capture the subtle changes in the CO<sub>2</sub> balance of the alpine permafrost, given that most of the present sites are in the central and eastern Tibetan Plateau. Long-term observations with regular maintenance and quality control of the eddy covariance data would provide solid proof to validate our finding that the uptake of CO<sub>2</sub> by plants will outpace the loss of CO<sub>2</sub> from permafrost and plant respiration on the Tibetan Plateau in the future. Long-term eddy covariance observations would also provide an opportunity for the scientific community to better understand the interannual variability in CO<sub>2</sub> exchange on the Tibetan Plateau, where the climate variability is significant, especially for precipitation. In situ observations should also cover abrupt changes (e.g., thermokarst collapse, thermokarst ponds/lakes and streams, including methane and nitrous oxide emissions) and complete the picture of how the variation in the net greenhouse gas balance of the alpine permafrost on the Tibetan Plateau will be altered by a changing climate. Integration of these in situ observations into Earth system models would benefit model development and help to better constrain the net greenhouse gas balance and its feedback to climate warming in the long term.

**Materials and Methods**

**Eddy Covariance Observations.** We obtained observations from 32 eddy covariance sites across the Tibetan Plateau. We obtained two types of CO<sub>2</sub>

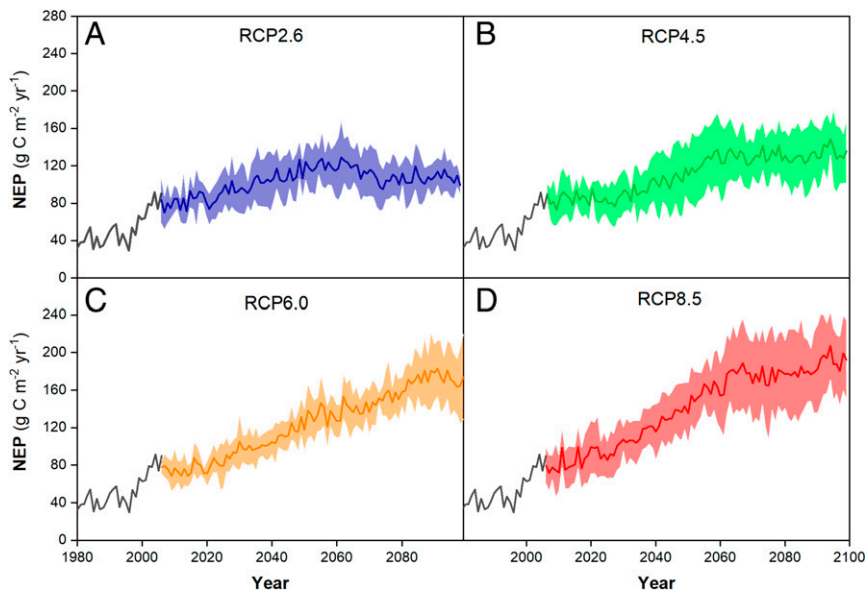


**Fig. 5.** Prediction of CO<sub>2</sub> exchange under a warming and wetting climate. Variation of the NEP during the last few decades and in the future under RCPs until the end of the current century: (A) RCP2.6, (B) RCP4.5, (C) RCP6.0, (D) RCP8.5. The solid curves are the ensemble mean of model simulations, and the shading represents  $\pm 1$  SD.

exchange data based on eddy covariance observations: raw data obtained by other researchers and literature-based data. The raw data were obtained by contacting the original researchers, whereas the literature-based data were obtained by searching the Web of Science (for English language papers, <http://apps.webofknowledge.com/>) and the China National Knowledge Infrastructure (for Chinese language papers, <https://www.cnki.net/>), using the following keywords: eddy covariance, alpine, carbon flux, Tibetan Plateau, and Qinghai-Tibetan Plateau. The eddy covariance sites covered all the ecosystems typical of this region: alpine shrublands (2 sites), alpine meadow (16 sites), alpine steppe (4 sites), alpine desert (1 site), and alpine wetland (9 sites). Most of the sites were in the central and eastern Tibetan Plateau. Eddy covariance sites are less common in the western and northern Tibetan Plateau as a result of the harsh climate and poor road access in these regions. A total of 10 sites were at altitudes of 3,000 to 3,500 m, 5 at 3,600 to 4,000 m, 7 at 4,000 to 4,500 m, and 5 at 4,500 to 5,000 m. Of these, 10 sites were characterized as continuous permafrost and the remaining 22 sites as noncontinuous permafrost. Data were obtained for a total of 77 site years across the Tibetan Plateau, an average of 2.4 y per site. Among them, 57 site years were conducted in the 2010s (2010 to 2020), accounting for three-quarters of the dataset. For continuous observations of more than 1 y, we calculated the multiyear average value for each site. The data presented here are therefore representative of the Tibetan Plateau in terms of the type of ecosystem, the altitude, and the state of the ground (i.e., continuous or noncontinuous permafrost), although there is a regional bias, with more sites in the east-central Tibetan Plateau.

Among the datasets, 10 of the eddy covariance sites were operated by the current authors, and these data are provided at 30- or 60-min intervals (Ali, Arou, Batang, Dashalong, Mt Everest, Muztag, NamCo, Shenzha, and Yakou), whereas the remaining data were obtained from peer-reviewed papers (SI Appendix, Table S1). Processing of the raw data followed the mainstream method adopted by previous studies across the Tibetan Plateau to guarantee consistency (47–50). We used eddy covariance data processing software (EddyPro, LI-COR Inc.) and TK3 to perform coordinate axis rotation and Webb–Pearman–Leuning correction. We used a positive net radiation to define the daytime flux, while a negative net radiation was classified as nighttime. After steady-state and integral turbulence characteristics tests on all the CO<sub>2</sub> flux data (47–50), the nighttime CO<sub>2</sub> exchange corresponding to a friction velocity ( $U^*$ )  $< 0.10$  to  $0.21$  m s<sup>-1</sup> was removed (site dependent, SI Appendix, Table S1) using the average values test approach of ChinaFLUX (51). The months from May (or late April) to September (or October) were defined as the growing season (SI Appendix, Table S1) and the remaining months as the nongrowing season (winter). Linear interpolation was used to reconstruct the CO<sub>2</sub> flux data missing within 2-h intervals. Data missing for more than 2 h were reconstructed based on the Michaelis–Menten light response relationship during the growing season:  $NEP = (\alpha \times PAR + A_{max}) /$

$(\alpha \times PAR + A_{max}) - RE$ , where  $A_{max}$  is the maximum rate of photosynthesis,  $\alpha$  is the apparent quantum yield, and RE is the ecosystem respiration. Data missing for more than 2 h during the nongrowing season were reconstructed using  $RE = a \times e^{bT}$ , where RE is ecosystem respiration,  $a$  and  $b$  are regression parameters, and  $T$  is the soil surface temperature. The daytime GPP during the growing season is the sum of the NEP and RE, whereas the NEP during the nongrowing season was considered to be the RE. Estimation of the daytime RE during GPP and RE partitioning in the growing season was obtained by the equation  $RE = a \times e^{bT}$ .

A similar procedure was applied for the literature-based data (SI Appendix, Table S1), and the daily CO<sub>2</sub> exchange rates were obtained using GetData Graph Digitizer 2.2.6 (<http://www.getdata-graph-digitizer.com>). All the sites in the 32 datasets were subjected to Webb–Pearman–Leuning density correction, and most sites were determined by the coordinate axis rotation approach, that is, two-dimensional (14 sites), three-dimensional (6 sites), or planar fit (6 sites) coordinate axis rotation. After quality control and screening of the data, the overall loss of data from these sites fluctuated between 8 and 48% (SI Appendix, Table S1).

**Analyses of Eddy Covariance Observations.** All the NEP data are displayed as mean  $\pm 1$  SE values unless stated otherwise. During the regional CO<sub>2</sub> budget estimation, site-averaged CO<sub>2</sub> exchange values were used to calculate an ecosystem average and then ecosystem-averaged CO<sub>2</sub> exchange rates and their corresponding extents were used to obtain a regional estimation, based on the 1:1,000,000 vegetation map of China (SI Appendix, Fig. S16) (37). The Van’t Hoff equation ( $y = ae^{bt}$ ) was used to calculate the temperature sensitivity ( $Q_{10}$ ) of CO<sub>2</sub> exchange ( $Q_{10} = e^{10b}$ , the 30-min or 1-h atmospheric temperature 2 m above ground observed by each site). Structural equation modeling (SEM) analysis was used to estimate the relative importance of direct and indirect impacts of geographical factors, climate factors, and soil processes on the spatial pattern of CO<sub>2</sub> fluxes. We hypothesized that geographical factors (altitude and latitude) would largely affect the climate factors (radiation, mean annual precipitation, and temperature), while climate factors would directly and indirectly regulate CO<sub>2</sub> exchanges via the SWC and mean annual ground temperature. During the SEM analyses, site-averaged CO<sub>2</sub> exchange (32 sites), geographical factors, climate factors, and soil factors were used. For SWC and mean annual ground temperature, they were extracted from each observation. For climate factors (shortwave downward radiation, mean annual precipitation and temperature), the data for the most adjacent pixel of each site was extracted from a high-resolution ( $0.1^\circ \times 0.1^\circ$ , 3-h steps) climatological dataset—namely, the China Meteorological Forcing Dataset (CMFD) (52). The CMFD was the first high spatiotemporal resolution gridded near-surface meteorological dataset developed specifically for land surface studies in China. It was constructed through the fusion of remote sensing products, reanalysis datasets, and about 700 meteorological stations of the

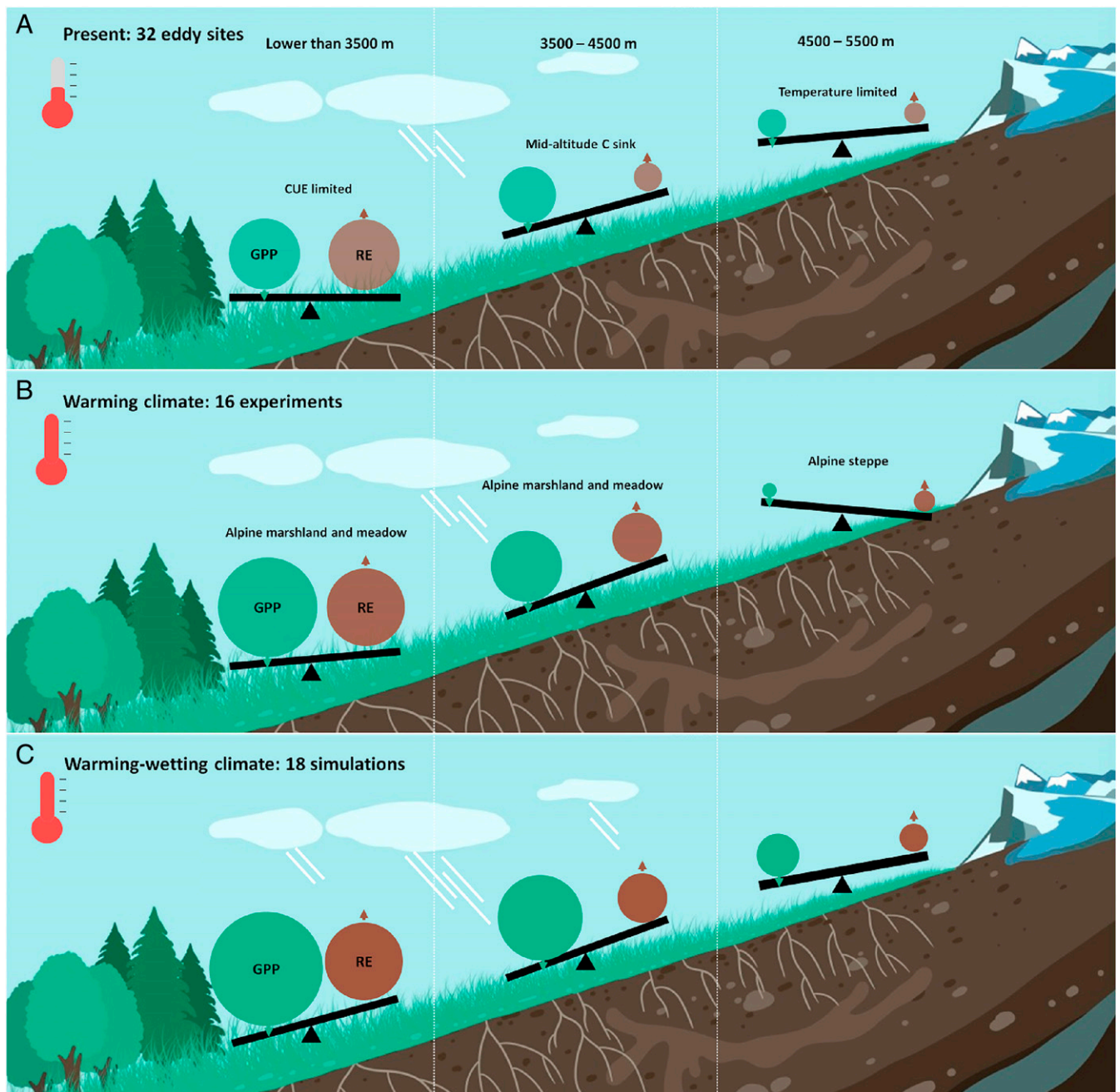


**Fig. 6.** Altitude-dependent pattern of CO<sub>2</sub> sinks and their feedbacks to climate change. The alpine ecosystem CO<sub>2</sub> sink on the Tibetan Plateau under (A) the present climate, (B) a warming-only climate, and (C) a warming-wetting climate. GPP, gross primary productivity; RE, ecosystem respiration; CUE, carbon use efficiency (NEP/GPP). A larger circle indicates a stronger CO<sub>2</sub> flux.

China Meteorological Administration. All SEM analyses were performed using IBM SPSS Amos 24.0.0 (SPSS Inc.).

**Additional Datasets for CO<sub>2</sub> Exchange.** Two additional datasets were compared with the CO<sub>2</sub> exchange across the Tibetan Plateau based on eddy covariance observations: FluxCom and MsTMIP. The FluxCom dataset is a newly published FluxNet-based upscaling dataset and provides temporally explicit estimates of the CO<sub>2</sub> and water fluxes derived from empirical upscaling eddy covariance measurements (31, 53). This dataset uses three independent machine learning approaches (artificial neural networks, multivariate adaptive regression splines, and random forests) for training on daily CO<sub>2</sub> fluxes based on 224 flux tower sites worldwide within FLUXNET and is driven by the CRUNCEPV6 dataset and satellite data. It is notable that only two sites were available on the Tibetan Plateau and included in the FLUXNET dataset. All three independent datasets

were used in this study. The CRUNCEPV6 dataset is based on a merged product of the Climate Research Unit observation-based monthly 0.5° climate variables and the 6-h resolution National Centers for Environmental Prediction reanalysis dataset (31). The FluxCom datasets of GPP, RE, and NEP were provided at a resolution of 0.5° during the period 1980 to 2013. During the comparison, we used the period 2000 to 2013 to compare the NEP of the FluxCom dataset with the estimation based on the eddy covariance observations.

The MsTMIP simulation is a formal multiscale synthesis, with prescribed environmental and meteorological drivers shared among model teams, and the simulations are standardized to facilitate comparison with other model results and observations through an integrated evaluation framework (the MsTMIP; *SI Appendix, Table S4*) (32). The MsTMIP simulations were classified into four groups (BG1, SG1, SG2, and SG3). The BG1 group was simulated by the time-varying climate, land use, and the deposition of CO<sub>2</sub> and reactive N

input (eight models). The SG1 group was simulated by the time-varying climate (14 models). The SG2 group was simulated by the time-varying climate and land use (14 models), and the SG3 group by the time-varying climate, land use, and CO<sub>2</sub> (14 models). All the models were driven by the Climate Research Unit–National Centers for Environmental Prediction climate data and the same soil map and were run at a resolution of 0.5° with monthly time steps.

**Manipulative Experiments.** A large number of manipulative experiments have been conducted across the Tibetan Plateau, particularly in the central and eastern Tibetan Plateau. The results of these experiments were obtained by searching the Web of Science (for English language papers, <http://apps.webofknowledge.com>) and the China National Knowledge Infrastructure (for Chinese language papers, <https://www.cnki.net>), using the following keywords: warming, alpine, carbon flux, Tibetan Plateau, and Qinghai-Tibetan Plateau. Given the important effects of rapid climate warming on plant physiology in such a high and cold area, we collected 16 manipulative warming experiments across all major ecosystem types. We only collected experiments in which the NEP was measured; some experiments in this region lacked observations of the net CO<sub>2</sub> balance—that is, they measured the above-ground biomass rather than the NEP (54). The manipulated experiments covered alpine marshlands, meadows, and steppe, and ranged from 3,200 to 4,900 m in altitude (more information in [Dataset S3](#)).

All the experiments were conducted using the open-top chamber method because there is a lack of electricity over most of the Tibetan Plateau (the experiments conducted with a closed-top chamber were excluded due to a severe effect on the measurement of precipitation). The warming rate ranged from 0.76 to 4.0 °C relative to the control treatment in terms of the annual average surface soil temperature. The magnitude of warming in these experiments was slightly lower but comparable with warming under the RCP 2.6 to 8.5 scenarios by the end of the present century (1.2 to 5.5 °C). Most of the experiments measured the SWC, which ranged from 5.2% in a dry meadow to 52.3% in a marshland. In total, 11 experiments were conducted with a single warming level (only a single warming treatment in addition to the control treatment), whereas 5 used a gradient-warming approach (more than two warming treatments in addition to the control treatment). All the warming treatments were conducted on a year-round basis, although the CO<sub>2</sub> exchanges were only measured during the growing season using transparent chambers coupled with a greenhouse gas analyzer (LI-COR 6400 or LI-COR 840A) as a result of the harsh climate, the lack of road access, and problems with field logistics during the winter months. Most of the studies were fairly short (i.e., less than 3 y), with only four sites observed for 3 y, indicating a lack of knowledge about their long-term response and feedback to future climate change.

Given that there is a possibility that warming changed a net CO<sub>2</sub> sink (a positive NEP) to a net CO<sub>2</sub> source (a negative NEP), the response ratio of the NEP ( $RR_{NEP}$ ) was calculated as  $RR_{NEP} = NEP_{Warming} / NEP_{Control}$ , where  $NEP_{Warming}$  is the average NEP under the warming treatment (usually 3 to 10 replicates), while  $NEP_{Control}$  indicates the average NEP under the control treatment (usually 3 to 10 replicates). Therefore,  $RR_{NEP} > 1.0$  indicates a positive effect of warming on the NEP, while  $RR_{NEP} < 1.0$  indicates the opposite ( $RR_{NEP} < 0$  suggests that the warming has changed the net CO<sub>2</sub> sink of an ecosystem to a net CO<sub>2</sub> source). The SD of  $RR_{NEP}$  was calculated using the equation  $V_{RR_{NEP}} = SD_{Warming}^2 / (n_{Warming} NEP_{Warming}^2) + SD_{Control}^2 / (n_{Control} NEP_{Control}^2)$ , where  $SD_{Warming}$  and  $n_{Warming}$  indicate the SD and number of replicates under the warming treatment, respectively;  $SD_{Control}$  and  $n_{Control}$  indicate the SD and the number of replicates under the control treatment, respectively.

The responses of  $RR_{NEP}$  to altitude, warming, and the SWC were fitted separately with a Bayesian linear mixed effect model using the Markov chain Monte–Carlo sampling method by the Bayesian Regression Models using ‘Stan’ package in R 4.0.3 (55). In this model, the site was set as the random effect factor to account for repeated measures within sites. All the model parameters were assigned default, uninformative priors. In each model, posterior summaries of the parameters were based on four independent chains of 5,000 samples each, of which the first 2,500 iterations were discarded as warm-up. We set the adapt-delta value (the target average proposal acceptance probability) to 0.99 and the maximum tree depth to 15 to eliminate any divergent transitions. The degree of convergence of the Markov chains was monitored using trace plots of the posterior samples and a Gelman–Rubin convergence statistic of <1.01 (56). A quadratic term was included to account for a possible nonlinear relationship between the variables. Model simplifications (a simple linear model versus a quadratic model) were conducted using the leave-one-out (LOO) information criterion. Models with a lower LOO value were considered to be better models, particularly if the difference in the LOO value between two models ( $\Delta LOO$ ) was more than twice the SE. Effects were considered as significant if the 95% credible intervals of the estimated parameter did not overlap with zero.

**Eddy Covariance Constraint on a Biogeochemical Model.** We developed a process-based model by coupling the eddy covariance dataset of the present study to an existing model to improve its performance. We used the Lund–Potsdam–Jena (LPJ) Dynamic Global Vegetation Model (57) and its successor, the LPJ–Wetland Hydrology and Methane (LPJ–WHyMe) model, which estimate and project the exchange of CO<sub>2</sub> in high-latitude and high-altitude permafrost regions (58). Snow accumulation, melting, and the depth dynamics of the active permafrost layer are explicitly represented in the LPJ–WHyMe model. We previously revised this model to apply it to simulate C exchange in the alpine ecosystems of the Tibetan Plateau (59). In the present study, we further constrained the model using the 32 eddy covariance sites to give regional estimations and projections.

We revised the plant functional types of the model to better represent the vegetation community of the alpine ecosystems across the Tibetan Plateau by adding six plant function types (alpine meadow, alpine steppe, alpine desert, alpine shrub, alpine wetland herbaceous, and alpine wetland dwarf plants) and improving their parameters based on a previous study (60). The plant functional types alpine wetland herbaceous and alpine wetland dwarf plants were used to represent *Kobresia littledalei* and *Kobresia pygmaea* within the hummock–hollow terrain marshlands on the Tibetan Plateau ([SI Appendix, Table S5](#)). The simulated vegetation types using the revised plant functional type parameters captured well the spatial pattern of the vegetation types based on the survey-based China Vegetation Atlas (1:1,000,000), the NEP magnitude, and seasonal variation ([SI Appendix, Figs. S16–S18](#)).

At the regional scale, a retrospective (1979 to 2005) run of the LPJ model was driven by soil texture, temperature, precipitation, clouds, and atmospheric [CO<sub>2</sub>]. We applied the Second National Soil Survey of China soil texture dataset (61) based on the classification scheme of the original LPJ soil texture map (58). The high-resolution CMFD (0.1° spatial resolution and 3-h temporal resolution) was used as the forcing data (52). Given the importance of soil water in driving the long-term variation in CO<sub>2</sub> exchange in semiarid and arid regions, we used the Global Land Evaporation Amsterdam Model soil moisture product (62) owing to its good data coverage in this region. We extracted a mask from the survey-based China Vegetation Atlas (1:1,000,000) to focus on the alpine ecosystems on the Tibetan Plateau. For the alpine marshlands, we used the Landsat-based remote sensing classification of marshlands in China. The 1 × 1 km resolution marshland maps were visually interpreted using Landsat products. During the model run, the first 10 y of climate data were used for a spin-up period of 1,000 y, and the run was performed at a resolution of 0.1°.

Prediction (2006 to 2100) of the CO<sub>2</sub> flux across the Tibetan Plateau was driven by outputs under four RCP scenarios from CMIP5 ([SI Appendix, Table S6](#)). The CMIP5 climate outputs include 11 model outputs for RCP2.6, 10 model outputs for RCP4.5, 7 model outputs for RCP6.0, and 18 model outputs for RCP8.5. Like the retrospective run, the projection runs of the model were driven by soil texture, temperature, precipitation, clouds, soil moisture, and atmospheric [CO<sub>2</sub>]. Each run of the LPJ model was performed at a different spatial resolution depending on the resolution of the climate forcing data of CMIP5 (0.75° × 0.75° to 3.75° × 3.75°). The soil texture maps and the land mask were therefore resampled to a different resolution to facilitate model simulation. During the prediction run, the first 10 y of climate data were used for a spin-up period of 1,000 y and run for 94 y (2006 to 2099).

**Data Availability.** All eddy-covariance-based CO<sub>2</sub> exchange observation and experimental warming data can be accessed in [Datasets S1–S3](#) as well as in the National Tibetan Plateau Data Center: <https://data.tpdc.ac.cn/en/disallow/15281316-4024-4409-8c0f-f91e2f5b6574> (63). All these data will be accessible upon publication.

**ACKNOWLEDGMENTS.** We thank the researchers at all stations across the Tibetan Plateau for their work under the harsh climate and efforts to make their datasets publicly accessible. Their contributions regarding the establishment and maintenance of the eddy covariance and manipulative experiments made this study possible. Dr. Shuang Zhong, Dr. Yafeng Wang, Dr. Jingxue Zhao, Dr. Ruiying Chang, Mr. Ming Hong, and Mr. Lai Wei are thanked for their help with this paper. We sincerely appreciate the editor and two reviewers for their contributions to this manuscript. This work was supported by the Strategic Priority Research Program of the Chinese Academy of Sciences (XDA20020401), the Second Tibetan Plateau Scientific Exploration (2019QZKK0404), the National Natural Science Foundation of China (41971145; 41671102), and the Youth Innovation Promotion Association of the Chinese Academy of Sciences (2020369). The FluxCom dataset was downloaded from <https://www.bgc-jena.mpg.de>. NASA’s Terrestrial Ecology Program (NNX11AO08A) funded MsMTIP Phase 1. During Phase 1, data management for MsMTIP was conducted by Modeling and Synthesis Thematic Data Center, with funding from NASA’s Terrestrial Ecology Program (NASA Grant NNH10AN681).



1. E. A. Davidson, I. A. Janssens, Temperature sensitivity of soil carbon decomposition and feedbacks to climate change. *Nature* **440**, 165–173 (2006).
2. G. Huguenin *et al.*, Estimated stocks of circumpolar permafrost carbon with quantified uncertainty ranges and identified data gaps. *Biogeosciences* **11**, 6573–6593 (2014).
3. IPCC, *Climate Change 2013: The Physical Science Basis. Contribution of Working Group I to the Fifth Assessment Report of the Intergovernmental Panel on Climate Change*, T. F. Stocker *et al.*, Eds. (Cambridge University Press, Cambridge, UK and New York, NY, 2013), pp. 1535.
4. A. H. MacDougall, C. A. Avis, A. J. Weaver, Significant contribution to climate warming from the permafrost carbon feedback. *Nat. Geosci.* **5**, 719–721 (2012).
5. C. D. Koven, D. M. Lawrence, W. J. Riley, Permafrost carbon-climate feedback is sensitive to deep soil carbon decomposability but not deep soil nitrogen dynamics. *Proc. Natl. Acad. Sci. U.S.A.* **112**, 3752–3757 (2015).
6. J. Z. Ding *et al.*, Decadal soil carbon accumulation across Tibetan permafrost regions. *Nat. Geosci.* **10**, 420–424 (2017).
7. E. A. G. Schuur *et al.*, The effect of permafrost thaw on old carbon release and net carbon exchange from tundra. *Nature* **459**, 556–559 (2009).
8. A. D. McGuire *et al.*, Variability in the sensitivity among model simulations of permafrost and carbon dynamics in the permafrost region between 1960 and 2009. *Global Biogeochem. Cycles* **30**, 1015–1037 (2016).
9. A. D. McGuire *et al.*, Dependence of the evolution of carbon dynamics in the northern permafrost region on the trajectory of climate change. *Proc. Natl. Acad. Sci. U.S.A.* **115**, 3882–3887 (2018).
10. B. K. Biskaborn *et al.*, Permafrost is warming at a global scale. *Nat. Commun.* **10**, 264 (2019).
11. E. F. Belshe, E. A. G. Schuur, B. M. Bolker, Tundra ecosystems observed to be CO<sub>2</sub> sources due to differential amplification of the carbon cycle. *Ecol. Lett.* **16**, 1307–1315 (2013).
12. S. Natali *et al.*, Large loss of CO<sub>2</sub> in winter observed across the northern permafrost region. *Nat. Clim. Chang.* **9**, 852–857 (2019).
13. A. D. McGuire *et al.*, An assessment of the carbon balance of Arctic tundra: Comparisons among observations, process models, and atmospheric inversions. *Biogeosciences* **9**, 3185–3204 (2012).
14. A. M. Virkkala *et al.*, Statistical upscaling of ecosystem CO<sub>2</sub> fluxes across the terrestrial tundra and boreal domain: Regional patterns and uncertainties. *Glob. Change Biol.* <https://doi.org/10.1111/GCB.15659>. (2021).
15. J. Obu *et al.*, Northern hemisphere permafrost map based on TTOP modelling for 2000–2016 at 1 km(2) scale. *Earth-Sci. Rev.* **193**, 299–316 (2019).
16. J. Ding *et al.*, The permafrost carbon inventory on the Tibetan Plateau: A new evaluation using deep sediment cores. *Glob. Change Biol.* **22**, 2688–2701 (2016).
17. D. F. Zou *et al.*, A new map of permafrost distribution on the Tibetan Plateau. *Cryosphere* **11**, 2527–2542 (2017).
18. X. X. Kuang, J. J. Jiao, Review on climate change on the Tibetan Plateau during the last half century. *J. Geophys. Res. Atmos.* **121**, 3979–4007 (2016).
19. M. X. Yang *et al.*, Permafrost degradation and its environmental effects on the Tibetan Plateau: A review of recent research. *Earth Sci. Rev.* **103**, 31–44 (2010).
20. Y. H. Ran, X. Li, G. D. Cheng, Climate warming over the past half century has led to thermal degradation of permafrost on the Qinghai-Tibet Plateau. *Cryosphere* **12**, 595–608 (2018).
21. M. X. Yang *et al.*, The Tibetan Plateau cryosphere: Observations and model simulations for current status and recent changes. *Earth Sci. Rev.* **190**, 353–369 (2019).
22. L. C. Huang *et al.*, Using deep learning to map retrogressive thaw slumps in the Beiluhe region (Tibetan Plateau) from CubeSat images. *Remote Sens. Environ.* **237**, 111534 (2020).
23. C. C. Mu *et al.*, Acceleration of thaw slump during 1997–2017 in the Qilian Mountains of the northern Qinghai-Tibetan plateau. *Landslides* **17**, 1051–1062 (2020).
24. L. Chen *et al.*, Determinants of carbon release from the active layer and permafrost deposits on the Tibetan Plateau. *Nat. Commun.* **7**, 13046 (2016).
25. T. Wang *et al.*, Permafrost thawing puts the frozen carbon at risk over the Tibetan Plateau. *Sci. Adv.* **6**, eaaz3513 (2020).
26. C. C. Mu *et al.*, Permafrost collapse shifts alpine tundra to a carbon source but reduces N<sub>2</sub>O and CH<sub>4</sub> release on the northern Qinghai-Tibetan Plateau. *Geophys. Res. Lett.* **44**, 8945–8952 (2017).
27. G. Zhang, Y. Zhang, J. Dong, X. Xiao, Green-up dates in the Tibetan Plateau have continuously advanced from 1982 to 2011. *Proc. Natl. Acad. Sci. U.S.A.* **110**, 4309–4314 (2013).
28. S. L. Piao *et al.*, Altitude and temperature dependence of change in the spring vegetation green-up date from 1982 to 2006 in the Qinghai-Xizang Plateau. *Agric. Meteorol.* **151**, 1599–1608 (2011).
29. D. Wei, H. Zhao, J. Zhang, Y. Qi, X. Wang, Human activities alter response of alpine grasslands on Tibetan Plateau to climate change. *J. Environ. Manage.* **262**, 110335 (2020).
30. X. Y. Wang *et al.*, Multisatellite analyses of spatiotemporal variability in photosynthetic activity over the Tibetan Plateau. *J. Geophys. Res. Biogeosci.* **124**, 3778–3797 (2019).
31. M. Jung *et al.*, Compensatory water effects link yearly global land CO<sub>2</sub> sink changes to temperature. *Nature* **541**, 516–520 (2017).
32. D. Huntzinger *et al.*, NACP M5TMIP: Global 0.5-deg Terrestrial Biosphere Model Outputs (version 1) in Standard Format, Data set. Available on-line [daac.ornl.gov] from Oak Ridge National Laboratory Distributed Active Archive Center, Oak Ridge, Tennessee (2018). <https://www.doi.org/10.3334/ORNLDAAC/1225>. Accessed 7 March 2019.
33. Q. L. Zhuang *et al.*, Carbon dynamics of terrestrial ecosystems on the Tibetan Plateau during the 20th century: An analysis with a process-based biogeochemical model. *Glob. Ecol. Biogeogr.* **19**, 649–662 (2010).
34. X. J. Lin *et al.*, Sensitivity of alpine grassland carbon balance to interannual variability in climate and atmospheric CO<sub>2</sub> on the Tibetan Plateau during the last century. *Global Planet. Change* **154**, 23–32 (2017).
35. S. L. Piao *et al.*, Impacts of climate and CO<sub>2</sub> changes on the vegetation growth and carbon balance of Qinghai-Tibetan grasslands over the past five decades. *Global Planet. Change* **98**, 73–80 (2012).
36. Z. N. Jin *et al.*, Net exchanges of methane and carbon dioxide on the Qinghai-Tibetan Plateau from 1979 to 2100. *Environ. Res. Lett.* **10**, 085007 (2015).
37. G. Yu *et al.*, High carbon dioxide uptake by subtropical forest ecosystems in the East Asian monsoon region. *Proc. Natl. Acad. Sci. U.S.A.* **111**, 4910–4915 (2014).
38. D. Wei *et al.*, Revisiting the role of CH<sub>4</sub> emissions from alpine wetlands on the Tibetan Plateau: Evidence from two *in situ* measurements at 4758 and 4320m above sea level. *J. Geophys. Res. Biogeosci.* **120**, 1741–1750 (2015).
39. C. Körner, *Alpine Treelines: Functional Ecology of the Global High Elevation Tree Limits* (Springer Science & Business Media, 2012).
40. Y. H. Yang *et al.*, Large-scale pattern of biomass partitioning across China's grasslands. *Glob. Ecol. Biogeogr.* **19**, 268–277 (2010).
41. L. Zhong *et al.*, Climate change trends and impacts on vegetation greening over the Tibetan Plateau. *J. Geophys. Res. Atmos.* **124**, 7540–7552 (2019).
42. L. Xiang *et al.*, Groundwater storage changes in the Tibetan Plateau and adjacent areas revealed from GRACE satellite gravity data. *Earth Planet. Sci. Lett.* **449**, 228–239 (2016).
43. B. Jia *et al.*, Interannual variations and trends in remotely sensed and modeled soil moisture in China. *J. Hydrometeorol.* **19**, 831–847 (2018).
44. Y. Q. Tian *et al.*, Carbon sequestration in two alpine soils on the Tibetan Plateau. *J. Integr. Plant Biol.* **51**, 900–905 (2009).
45. M. Wörner *et al.*, Higher recent peat C accumulation than that during the Holocene on the Zoige Plateau. *Quat. Sci. Rev.* **114**, 116–125 (2015).
46. C. Y. Liu *et al.*, Year-round measurements of nitrous oxide emissions and direct emission factors in extensively managed croplands under an alpine climate. *Agric. Meteorol.* **274**, 18–28 (2019).
47. E. Falge *et al.*, Gap filling strategies for defensible annual sums of net ecosystem exchange. *Agric. For. Meteorol.* **107**, 43–69 (2001).
48. M. Reichstein *et al.*, Ecosystem respiration in two Mediterranean evergreen Holm Oak forests: Drought effects and decomposition dynamics. *Funct. Ecol.* **16**, 27–39 (2002).
49. L. Wang *et al.*, Water and CO<sub>2</sub> fluxes over semiarid alpine steppe and humid alpine meadow ecosystems on the Tibetan Plateau. *Theor. Appl. Climatol.* **131**, 547–556 (2018).
50. G. S. Campbell, J. M. Norman, *An Introduction to Environmental Biophysics* (Springer Science & Business Media, 2012).
51. H. Q. Li *et al.*, Seasonal and inter-annual variations in CO<sub>2</sub> fluxes over 10 years in an alpine shrubland on the Qinghai-Tibetan Plateau, China. *Agric. Meteorol.* **228**, 95–103 (2016).
52. J. He *et al.*, The first high-resolution meteorological forcing dataset for land process studies over China. *Sci. Data* **7**, 25 (2020).
53. M. Jung *et al.*, Scaling carbon fluxes from eddy covariance sites to globe: Synthesis and evaluation of the FLUXCOM approach. *Biogeosciences* **17**, 1343–1365 (2020).
54. Y. Yang *et al.*, Permafrost and drought regulate vulnerability of Tibetan Plateau grasslands to warming. *Ecosphere* **9**, e02233 (2018).
55. P. Bürkner, An R package for bayesian multilevel models using Stan. *J. Stat. Softw.* **80**, 1–28 (2017).
56. A. Gelman, J. Hill, *Data Analysis Using Regression and Multilevel/Hierarchical Models* (Cambridge University Press, 2006).
57. S. Sitch *et al.*, Evaluation of ecosystem dynamics, plant geography and terrestrial carbon cycling in the LPJ dynamic global vegetation model. *Glob. Change Biol.* **9**, 161–185 (2003).
58. R. Wania, I. Ross, I. Prentice, Implementation and evaluation of a new methane model within a dynamic global vegetation model: LPJ-WHYMe v1.3.1. *Geosci. Model Dev.* **3**, 565–584 (2010).
59. D. Wei, X. D. Wang, CH<sub>4</sub> exchanges of the natural ecosystems in China during the past three decades. *J. Geophys. Res. Biogeosci.* **121**, 2169–8953 (2016).
60. Q. Gao *et al.*, Climate change and its impacts on vegetation distribution and net primary productivity of the alpine ecosystem in the Qinghai-Tibetan Plateau. *Sci. Total Environ.* **554–555**, 34–41 (2016).
61. W. Shangquan *et al.*, A China data set of soil properties for land surface modeling. *J. Adv. Model. Earth Syst.* **5**, 212–224 (2013).
62. B. Martens *et al.*, GLEAM v3: Satellite-based land evaporation and root-zone soil moisture. *Geosci. Model Dev.* **10**, 1903–1925 (2017).
63. D. Wei *et al.*, Data of "A literature-based eddy covariance carbon exchange dataset on the Tibetan Plateau". National Tibetan Plateau Data Center. <https://data.tpdc.ac.cn/en/disallow/15281316-4024-4409-8c0f-f91e2f5b6574>. Accessed 15 July 2021.